A Framework For Robot-Assisted Doffing of Personal Protective Equipment

Antonio Umali[1] and Dmitry Berenson[2]

***Abstract*— When treating highly-infectious diseases such as Ebola, health workers are at high risk of infection during the doffing of Personal Protective Equipment (PPE). This is due to factors such as fatigue, hastiness, and inconsistency in training. The introduction of a semi-autonomous robot doffing assistant has the potential to increase the safety of the doffing procedure by assisting the human during high-risk subtasks. However, using a robotic assistant requires transforming a purely human task into a sequence of safe and effective human-robot collaborative actions. Since diseases like Ebola can spread through the mucous membranes of the face our goal in synthesizing these actions is to keep the human's hands away from his or her face as much as possible. As a secondary goal, we also seek to minimize the human's effort. We segment the doffing procedure into a sequence of human and robot actions such that the robot only assists when necessary and the human performs the more intricate parts of the procedure. Our framework then synthesizes assistive motions for the robot that perform parts of the tasks. Our experiments on five doffing tasks suggest that the introduction of a robot assistant improves the safety of the procedure in three out of four of the high-risk doffing tasks while reducing effort in all five tasks.**

I. Introduction

One of the most dangerous steps in the process of treating highly-infectious diseases like Ebola is the doffing of Personal Protective Equipment (PPE) worn by health-care workers who interact with infected patients and contaminated facilities. According to the Center for Disease Control (CDC), the removal of used PPE is "a high-risk process that requires a structured procedure, a trained observer, and a designated area for removal to ensure protection. PPE must be removed slowly and deliberately in the correct sequence to reduce the possibility of self-contamination or other exposure to Ebola virus" [1]. Because the doffing process involves numerous steps (24 steps in the most recent guidelines [1]) and must be repeated often under stressful conditions, it poses a significant risk of infection for health-care workers.

This paper presents a method that seeks to enable less-risky and less-strenuous doffing by using a human-supervised dual-arm manipulator (Baxter) to assist with the process (e.g., Figure 1). We propose a framework to synthesize motions for helping in the removal of certain pieces of PPE while reducing the risk of infection to the human and reducing the effort required to perform the task. The robot performs the doffing task in collaboration with the human, either by holding the PPE in a key position while the human removes a body part from inside it (which we call *support* motion) or by removing the PPE from the human's body itself (which we call *transfer* motion). Since many infectious diseases (including Ebola) can be spread through the mucous membranes of the eyes, ears, nose, and mouth, we synthesize support and transfer motion so as to maximize the distance between the worker's hands and his or her face during the doffing process. A secondary goal is to assist with doffing in a way that is not strenuous for the human (we measure strain using the RULA [2] and REBA [3] metrics). Finally, we aim to make robot's motion as intuitive for the human as possible while considering the above metrics. Note that the robot executes its motion for each step of the procedure autonomously but, for safety, an operator supervises the robot. The operator decides when the robot and human are ready to advance to the next step and which motion, out of a small set of autonomously planned motions, it should use.

Fig. 1: Baxter helping in the removal of the apron.

We compared the performance of robot-assisted doffing against unassisted doffing in five PPE component removal tasks. Our experiments suggest that assisted doffing lessens the average risk of infection in three out of four high-risk tasks. Furthermore, assisted doffing reduced the average effort exerted by subjects in all of the tasks.

II. Related Work

Recent compliant robots, such as Baxter, have allowed robots to interact with humans in close proximity. Several researchers have explored using robots as household companions and assistants [4], [5]. However, these works did not perform collaborative manipulation with the human. [6] presented a framework based on imitation and reinforcement

[1] Worcester Polytechnic Institute, Worcester, MA, USA (avumali@wpi.edu). [2] University of Michigan, Ann Arbor, MI, USA (berenson@eecs.umich.edu). This work was supported in part by NSF grants IIS-1317462, IIS-1514649, and IIS-1656101.

learning for learning to generate robot motions for collaborative manipulation tasks with humans. However, their work focused on the manipulation of rigid objects and did not have the robot and the human in very close proximity, as we do in this work.

Recent work has explored the use of a robot to assist in upper-body dressing for humans with movement limitations [7]. Gaussian Mixture Models were used to model the movement of the user's upper body enabling the user to move into the clothing while the robot holds it still. [8] also addressed the problem of dressing by creating primitive actions which constitute complex motions in human dressing. Using these, they were able to create a simulation and animation of how humans put on pieces of clothing. Furthermore, they were able to identify robotics-oriented properties such as grasp points, end-effector motion, and release motions. Shinohara et al. proposed using reinforcement learning to learn motor skills necessary to interact with non-rigid materials [9][10]. They focused on the topological relationship between the robot's configuration and material, simplifying the problem by assuming that fine details about the material (e.g. wrinkles) are irrelevant to perform most tasks. Yamazaki et al. [11] focused on developing a vision-based state-estimator for the materials and learning the mappings between robot motions and material states and were able to perform lower-body dressing on a mannequin. While these works present ideas which may be beneficial to our problem, they are both highly dependent on obtaining accurate perception of the object using computer vision, which is very difficult in real-world scenarios with cloth that can be occluded. In contrast, our approach relies on the human's ability to perceive the clothing thus we do not require vision data.

Learning from Demonstration (LfD) [12] is a common approach for synthesizing robot motions from human demonstrations. LfD has been used in robotics for the generation of control policies in tasks such as biped walking [13] and grasping [14]. However, LfD is difficult to use in human-robot interaction tasks because the policies will change depending on the person the robot is working with. In this work, we use demonstration motions as an initial guide for removing a piece of PPE but the path can be changed by an optimizer to meet constraints (e.g. reachability).

Our method requires generating a robot trajectory that is similar to a human's demonstration. Several trajectory optimization methods exist for this kind of task [15] [16][17]. The TrajOpt [15] method we use has been shown to work well with high degree-of-freedom problems and generates plans quickly even when complex constraints and cost functions are present.

III. Definitions

A configuration of the human is defined as $q_h \in Q_h$, we use different human models with different numbers of degrees of freedom according to which PPE component is being considered. The configuration of the robot is $q_r \in Q_r$. To address the complexity that deformable objects introduce into state definition and estimation as well as to motion planning, specifically for manipulation [18], we make the assumption that the PPE models we receive as input are composed of rigid parts; i.e. a (articulated) rigid body. We can then define the state of a PPE component in terms of its pose $T_{ppe} \in SE(3)$.

IV. Classifying and Quantifying Human Motions

Before discussing our framework for robot-assisted doffing, we introduce key concepts that will be used to classify and evaluate human motion in the framework. We also present metrics which evaluate these motion classes with respect to their overall safety. These metrics will later be used in generating a predicted human motion and in comparing the final human-robot motions to the original demonstration.

A. Classification

We classify demonstrated human motion according to the changes in the state of both the PPE and the human. Motions are divided into three classes:

1) *Transfer Motion*—where the body part, which the PPE component being doffed is attached to, remains in a nearly-static pose throughout the motion while the PPE component undergoes changes that lead to it being detached from the person. E.g., removing the goggles from the head.
2) *Support Motion*—where the PPE component remains in a nearly-static state while the person moves the attached body part away from it. E.g., taking the foot out of the boot.
3) *Adjustment Motion*—where the PPE component, the attached body part, or both undergo a series of small rapid movements. E.g. removing the inner gloves.

We observed that doffing motions performed by humans are usually neither pure transfer nor support motions; they are sequences of adjustment motions with either dominant transfer or support characteristics. This means that to preserve the human's behavior the robot would need to move simultaneously with the human. This makes generating robot motion very difficult because we do not know how the human will react and the robot must sense and move quickly to compensate. Instead, in our framework we convert adjustment motions to transfer and support motions so that the robot and human do not need to move simultaneously.

B. Assessing Human Motion Quality

To ensure that the new sequence of actions has less risk and effort than the original one, we propose the use of several metrics which represent how much risk an action carries. The first metric considers the distance between the worker's hands and their face, which is important because the hands perform tasks that expose them to harmful agents (e.g. handling infected materials, touching patients, etc.). The hands-to-face metric thus aims to capture the risk of contamination during a doffing task. For planning purposes, we can directly compute the distance of the human model's hands to its face in simulation. However in the physical

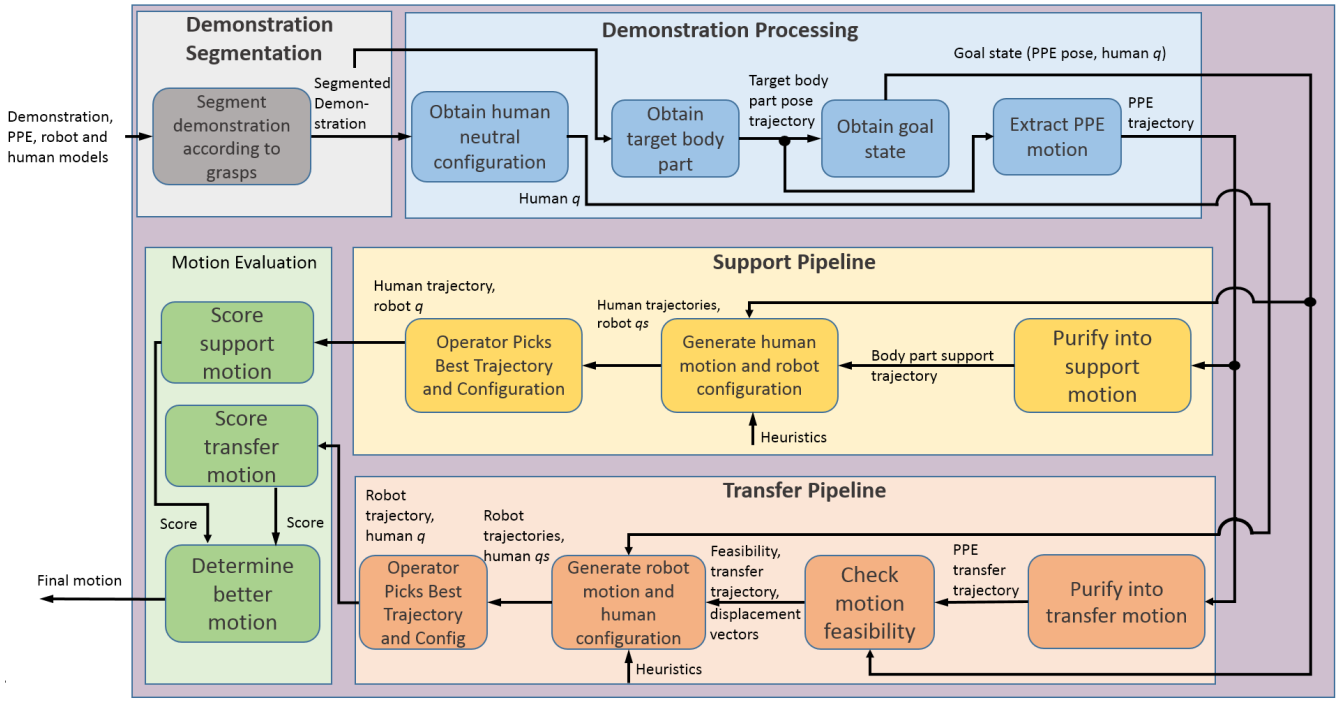

Fig. 2: Diagram showing the robot-assisted doffing framework. After segmenting and processing the demonstration trajectory, we run the support pipeline and transfer pipeline which generate candidate motions for robot-assisted removal. The motion evaluation section determines which motion is best and sends it to the robot.

environment this distance can be computed from point-cloud data gathered by the Kinect sensor:

$$FD(q_h) = \min_{i,j}(d(\text{face}_{q_h}[i], \text{hands}_{q_h}[j])), \tag{1}$$

where d is the Euclidean distance function, face_{q_h} and hands_{q_h} are arrays representing the location of geometries (solid bodies in simulation or point clouds in execution) for their respective body parts. We then compute the sum of all the positive differences between these distances above a threshold ϵ_d across all frames. We filter out distances from actions which can be deemed low-risk and increase the penalty for actions which can be considered high-risk (with respect to infection probability) using a quantity we call the *Hands-to-Face Distance Score*:

$$\lambda(\tau_h) = \sum_{i=1}^{|\tau_h|} max(\epsilon_d - FD(\tau_{h,i}), 0)). \tag{2}$$

Lower values of λ represent better infection safety.

We also aim to reduce the overall effort exerted by the worker during the doffing procedure. For this we use the Rapid Upper Limb Assessment (RULA)[2] and Rapid Entire Body Assessment (REBA)[3], which are methods used to quickly evaluate the effort of a given human configuration. In the doffing procedure low-strain postures are expected and unavoidable, and we do not want to them to influence the effort score. Instead we will capture the effect of postures with a significant strain using this effort scoring function:

$$E(\tau_h) = \sum_{i=1}^{|\tau_h|} max(R(\tau_{h,i}) - \epsilon_e, 0)m_i, \tag{3}$$

where $\tau_{h,i}$ is the ith posture being held by the subject, ϵ_e is an effort score which represents the minimum effort we want to be considered as significant, m_i is the amount of time the ith posture is held, and R is the REBA function. This scoring function allows us to filter out postures which can be considered negligible effort using ϵ_e. Lower values of E signify that less significant effort was exerted during the task.

V. FRAMEWORK OVERVIEW

Due to the difficulty of having the robot and human move simultaneously, we have created a framework that decomposes a doffing task into a sequence of human or robot actions and then plan robot motions which best assist the human. The framework (see Figure 2) takes as input the task demonstration represented by the human trajectory τ_h and PPE component trajectories in τ_{ppe}. Each trajectory is represented as a discrete sequence of n waypoints. The framework has five major blocks:

A. Demonstration Segmentation

We use changes in the grasp of the PPE to partition a complex task into a series of sub-tasks. Because accurate detection of human grasps is not within the scope of this work, we perform this segmentation manually.

B. Demonstration Processing

To avoid the problem of adapting to the human's reactions, the motion of the PPE component is purified into support and transfer motions. Let the human's body be discretized into a set of rigid bodies H, the target body part b is the

one with the greatest cumulative displacement from the PPE component during a demonstration:

$$b = \underset{h \in H}{\operatorname{argmin}} \left(\sum_{i=1}^{|\tau_h|} |\mathbf{t}_{ppe,i} - \mathbf{t}_{h,i}| \right), \tag{4}$$

where $\mathbf{t}$ represents a 3×1 translation vector and i is the index of a point in the trajectory. Using b, we define the goal state as the pose of the PPE component in b's frame at the end of the demonstration: $T_{b,n}^{ppe}$. The motion of the PPE component relative to b is then used to obtain the change in pose of the PPE component (transfer) or b (support).

These motions are used to consider either moving the PPE component along a smooth trajectory (transfer) or keeping its pose static (support). As the robot performs either of these, the human will be able to make adjustment motions. This block outputs two trajectories; one for the PPE component and the other for b, which will be used to generate robot and expected human motions.

C. Transfer Pipeline

This block generates a human configuration and robot trajectory corresponding to the doffing motion where the human holds a static posture and the robot removes the PPE component from the human. To do this, we first discretize the space of human standing poses (a 2-dimensional xy grid and discretized angles of rotation about the z-axis). We then apply the transform of each standing pose to the entire trajectory and check if all the points have valid Inverse Kinematics (IK) solutions for one or both (depending on the task) of the robot's manipulators. We output all such feasible trajectories.

If no standing pose allowing a feasible trajectory is found this block computes a set of closest-fit τ_r trajectories (using a Jacobian-based, gradient-descent IK method) and the set of standing poses for which the start and end transforms of the adjusted transfer motion are reachable. New transfer motions τ_r, which will allow the robot to remove the PPE from a nearly-motionless human, are generated using motion planning by trajectory optimization (Section VI) with the closest-fit trajectories and feasible transformations as input. This component also generates the configuration which the human must hold while the robot removes the PPE from his or her body. Since we do not model the human and PPE with high accuracy, we require an operator-in-the-loop to select which trajectory will be best suited for the current doffing task during execution.

D. Support Pipeline

This block generates an expected human trajectory and robot configuration corresponding to the doffing motion where the robot holds a PPE component in place and the human moves out ofthe PPE component. This block performs trajectory optimization (Section VI) to create a new support motion for the human. It also uses the first transform of the trajectory to generate a static robot configuration, using inverse kinematics, for the robot which will be used to hold the PPE in place. The robot will grasp the PPE upon the human's command, once the human places the appropriate parts of the PPE in the robots gripper(s). We again used an operator to select the best trajectory for the doffing task.

E. Motion Evaluation

This block uses metrics to assign a scalar-valued score to the motion and compares the generated transfer and support motions to determine which of them should be used for the task. The human's trajectory is evaluated using the manipulability metric MS defined in Section VI. The overall score of a motion is then:

$$S(\tau_r, \tau_h) = E(\tau_h) + \lambda(\tau_h) + \frac{1}{MS(\tau_r)}. \tag{5}$$

The motion with the lowest S value is the one used to doff the PPE component.

VI. TRAJECTORY OPTIMIZATION

In this section, we describe how we generate transfer and support motions for both the human and the robot using the TrajOpt [15] trajectory optimizer. TrajOpt's flexibility in specifying constraints and cost functions allows us to use our motion assessment metrics as well as giving us the freedom to insert other metrics which enable us to generate appropriate plans in the presence of a human. Robot motions are planned for transfer motions while human motions are planned to create an expected motion for the human for support motions.

A. PPE Simulation

Simulating the motion of the PPE accurately would provide the best accuracy when determining segmentation points as well as provide collision information to our planner. The difficulty in simulation lies in properly representing the object's physical parameters (e.g. stiffness, friction, etc.) [19] [20] [21], which we do not assume are available. To address this problem, we use a conservative geometric representation of the PPE as a chain of rigid bodies. We also assume that once the robot has grasped the PPE, it is rigidly attached to the end-effector(s). We do these for two reasons: (1) This allows us simulate the moving parts of the PPE by adding them as joints. For example, the strap on the goggles was treated as a prismatic joint which collapses when it is not in contact with the human. (2) This allows us perform collision checking using distance computation [22] in TrajOpt

B. Change-point identification

We observed that for portions of the demonstration where the PPE component is detached from the human, there should be more freedom in planning the robot motions. For example, once the PPE is removed, the robot need not follow the demonstrated path in order to dispose of the PPE. Thus we segment the input trajectory into two phases: the removal phase and the placement phase. These phases are separated at the point where the PPE component is considered to be removed from the person. This point is determined by running the demonstration in our simulator and finding the

point in the trajectory where there are changes to the PPE component's state (e.g. the goggles' strap has snapped off the head).

In the event of there being multiple phase separation points, we take the point with the lowest index. Trajectory optimization is then performed at each of these phases, with all of the costs applied to the first (removal) phase and only Legibility (defined below) for the second (placement) phase. The resulting trajectories from each phase are concatenated to produce the final trajectory.

Within each phase, we segment again to determine critical points in the motion. These are points where the translation of the PPE significantly changes direction.

$$x_{prev,i} = \mathbf{t}_{ppe,i} - \mathbf{t}_{ppe,i-1} \tag{6}$$

$$x_{next,i} = \mathbf{t}_{ppe,i+1} - \mathbf{t}_{ppe,i} \tag{7}$$

$$\rho_{x_i} = \arccos\left(\frac{x_{prev,i} \cdot x_{next,i})}{\|x_{prev,i}\|\|x_{next,i}\|}\right) \tag{8}$$

$$\psi_{x_i} = \arctan 2(\sin(\rho_{x_i}), \cos(\rho_{x_i})), \tag{9}$$

where ρ is the angle between the vectors $x_{prev,i}$ and $x_{next,i}$ and ψ is that angle constrained to the set $[-\pi, \pi]$. We define a significant change in direction to be when ψ_{x_i} exceeds a threshold ϵ_a. We also check for points where the linear or angular velocity of the motion undergoes a significant increase or decrease, i.e. a change exceeding a threshold ϵ_v.

The poses of the PPE during these critical points, along with the goal state pose, are then considered to be pose constraints on the PPE component and are used as pose constraints for the end-effector path (i.e. the robot should move the PPE through these critical points in its path).

C. Robot planning costs

We assign a pose-space deviation cost to the generated robot motions to minimize deviation from the demonstration motion. This cost, denoted Ω, is the difference of the ith planned trajectory point's pose between the target body part b and the PPE and the ith demonstration point's relative pose between the same objects:

$$DP(\mathbf{T}_a, \mathbf{T}_b) = \begin{bmatrix} \mathbf{t}^{\mathbf{T}_a}_{\mathbf{T}_b} \\ \arctan 2(\mathbf{R}^{\mathbf{T}_a}_{\mathbf{T}_b 32}, \mathbf{R}^{\mathbf{T}_a}_{\mathbf{T}_b 33}) \\ -\arcsin(\mathbf{R}^{\mathbf{T}_a}_{\mathbf{T}_b 31}) \\ \arctan 2(\mathbf{R}^{\mathbf{T}_a}_{\mathbf{T}_b 21}, \mathbf{R}^{\mathbf{T}_a}_{\mathbf{T}_b 11}) \end{bmatrix} \tag{10}$$

$$\Omega(\tau_p, \tau_d, i) = |\|DP(\text{PPE}_{\tau_{p,i}}, b_{\tau_{p,i}})\| - \tag{11}$$

$$\|DP(\text{PPE}_{\tau_{d,i}}, b_{\tau_{d,i}})\|, \tag{12}$$

where τ_p denotes the planned trajectory, τ_d denotes the demonstration trajectory, and DP denotes pose difference between two transforms ($\mathbf{t}$ is the translation vector and $\mathbf{R}$ is the rotation matrix). We also add a cost which penalizes deviation from the curvature of the demonstration. We calculate ψ_{x_i} and $\psi_{x_{d_i}}$, for each point from the planned and demonstration trajectories, respectively. The cost is then

$$\zeta(x_i) = |\psi_{x_i} - \psi_{x_{d_i}}|. \tag{13}$$

For two-arm planning, we calculate $\zeta(x_i)$ for the end-effector points of each arm and take the sum as the cost.

We use the manipulability measure [23] to bias the trajectory away from singularities. Given a trajectory τ_r the manipulability MS is:

$$M(q_r) = \sqrt{det(J(q_r)J(q_r)^T)} \tag{14}$$

$$MS(\tau_r) = \sum_{i=1}^{|\tau_r|} M(\tau_{r,i}), \tag{15}$$

where M calculates the manipulability of a configuration, $J(q_r)$ is the Jacobian of the robot's end-effector at q_r. For two-arm planning, we calculate the manipulability of each arm and take the sum as the score.

It is also easier for the human to cooperate with the robot if they know what to expect from the robot's motion. Dragan et al. formalized notions of motion predictability and legibility [24]. They proposed mathematical models for these based on the principle of rational actions and used these models to generate legible motion for a robot using trajectory optimization [25]. Given a trajectory τ and a single goal q_{goal}, we compute motion legibility $L[\tau]$ as:

$$C[\tau] = \frac{1}{2}\int \left(\frac{d\tau(t)}{dt}\right)^2 dt \tag{16}$$

$$P(G|\tau_{q_{\text{start}} \to q}) = \frac{\exp(-C[\tau_{q_{\text{start}} \to q}] - C[\tau^*_{q \to q_{\text{goal}}}])}{\exp(-C[\tau^*_{q_{\text{start}} \to q_{\text{goal}}}])} \tag{17}$$

$$L[\tau] = \frac{\int P(G_R|\tau_{q_{\text{start}} \to \tau(t)})(T-t)dt}{\int (T-t)dt}, \tag{18}$$

where $C[\tau]$ is a cost function that computes the sum-squared velocity of τ and $\tau^*_{q_1 \to q_2}$ is the optimal trajectory from q_1 to q_2 under C. We use L as a cost function during our placement phase to keep our trajectories smooth as well as communicate to the human that the PPE is being placed away from them.

D. Robot closed-chain kinematics constraint (two arm tasks)

Two-arm planning tasks involve maintaining a kinematic closure constraint which preserves the pose between the robot's end-effectors. To impose this constraint, we use the idea of active and passive sub-chains [26]: The first arm is unconstrained, while the second is constrained to maintain a fixed end-effector transform to the first arm's end-effector.

E. Human planning cost functions

To generate expected human motion we used hands-to-face distance score as a cost to prevent excessive arm movement, thus biasing most of the movement to the torso kinematic chain. We wish to also use the REBA cost R to minimize the effort. However, the problem with R is that there is no well-defined gradient (which is necessary for TrajOpt); scores are defined on a series of if-else blocks with various ranges for the joint values. Thus, to obtain a gradient, we modify our computation of the REBA cost for planning purposes.

We observed that the REBA metric divides a human's configuration space into equal-cost subspaces. I.e. the R function produces a set of cost plateaus in Q_h. Within a plateau the gradient of R is zero, thus TrajOpt will not be able to move a configuration within or out of a subspace. Thus we change

the cost function such that it varies throughout the subspace should the subspace not be the optimal one (not having the lowest R score possible). This new cost function, which we call the boundary distance score BS, assigns the cost of a point to be the distance to the boundary of the closest adjacent subspace of least-cost (see Fig. 3). We describe how to compute BS below:

Let the human's configuration space Q_h be partitioned into a set of axis-aligned bounding boxes $\mathcal{B} = \{\square_1, \square_2, ...\}$. The bounds of the boxes in $\mathcal{B}$ are defined by the REBA scoring process, which also assigns a score to each box. The REBA score of a configuration is the same for any configuration inside a box; i.e. $R(q_{h,1}) = R(q_{h,2})$ if $q_{h,1}, q_{h,2} \in \square_i$.

Let $\square_{q_h} \in \mathcal{B}$ be the box that contains q_h. Let $\mathcal{A}_{\square_{q_h}} \subseteq \mathcal{B}$ be the set of boxes adjacent to $\square_{q_h}$. We can then define the set of lowest-cost boxes adjacent to $\square_{q_h}$ as:

$$\mathcal{A}^*_{\square_{q_h}} = \{\square_i \in \mathcal{A}_{\square_{q_h}} \,|\, R(\square_i) = \min_{\square_j \in \mathcal{A}_{\square_{q_h}}} R(\square_j)\}. \quad (19)$$

Let $d(q_h, \square_i) \in \mathbb{R}$ be the distance between configuration q_h and the boundary of $\square_i$. $d(q_h, \square_i) = 0$ if $q_h \in \square_i$. Then BS is:

$$BS(q_h) = \min_{\square_i \in \mathcal{A}^*_{\square_{q_h}}} d(q_h, \square_i). \quad (20)$$

TrajOpt then uses the numerical gradient of BS with the differentiation step size ϵ_c to minimize the effort of an expected human motion.

VII. Results

A. Experiment Setup

To verify our hypothesis that a robot assistant can make the doffing procedure safer and less strenuous for the human, we conducted an experiment where 10 volunteers (7 male, 3 female, ages 18-30) performed the doffing procedure with and without the robot. None of the participants had previously performed the doffing procedure. We focused on the doffing of five separate PPE components: the apron, goggles, faceshield, hood, and coverall. Each subject was required to don the complete PPE to simulate an actual field deployment scenario.

For the unassisted doffing, subjects were instructed to remove the components of the PPE in a specific order, taking great care to follow the CDC guidelines [1]. If a component of the PPE was mishandled the entire process was repeated. For the robot-assisted doffing, we used Rethink Robotics' Baxter robot equipped with two parallel grippers for some tasks and a single vacuum gripper for others. Subjects are instructed to avoid touching their face during the entire doffing procedure. A kill switch was used to stop the robot in case of an emergency. To ensure that the proper actions are taken during both assisted and unassisted doffing procedures, each subject was trained by watching a series of videos detailing the proper donning of the PPE, the CDC guidelines for PPE doffing, and the steps and removal phases in the robot-assisted doffing. Subjects practiced these procedures until they were done correctly. After training, the subjects performed doffing once with the robot and once without

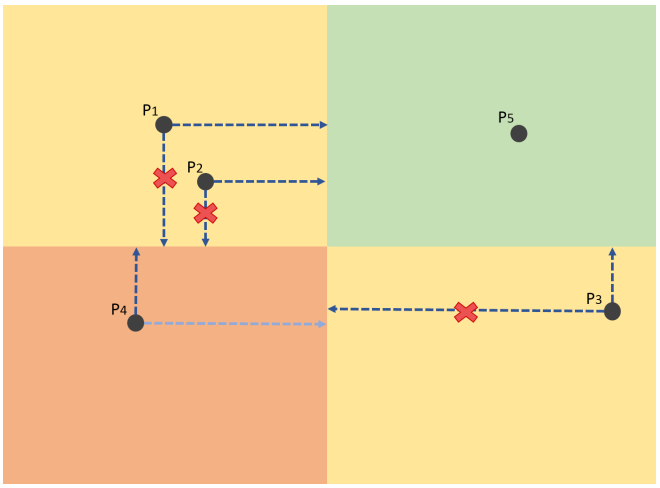

Fig. 3: 2D example of how the REBA metric partitions the human configuration space. The orange box has the highest effort score, followed by the yellow boxes, and then the green box. P1 and P2 are two points in the same box and their gradients point in the same direction. P4 shows how we assign a cost should there be two adjacent boxes with equivalent better scores, with the dark blue arrow indicating a smaller distance as compared to the light blue arrow. The x's on the arrows show that we do not consider adjacent boxes that are higher cost.

and each trial was recorded. Subjects were observed by four cameras: two webcams, an audio-visual camera, and a Microsoft Kinect2.

B. Algorithm Setup

The constants in our algorithms were defined as $\epsilon_a = 15°$, $\epsilon_d = 0.1$m, and $\epsilon_e = 7$ REBA units, the maximum score a posture can get before being deemed high-effort [3]. For reachability checking, we use a grid cell size of 0.05m and θ discretization of $\pi/4$. We disregarded x and y displacements greater than 0.6m and 0.3m from the robot, respectively, as well as θ displacements where $|\theta| \leq \pi/4$. For trajectory optimization, $\epsilon_c = 1e^{-5}$ and we used a joint-velocity cost coefficient of 250, a continuous collision cost coefficient of 500, and a discrete collision coefficient cost of 250—only for the placement phase (these are standard cost functions available in TrajOpt). For our cost functions, we used coefficients of 375 and 125 the translation and rotation components of Ω, respectively, 50 for ζ, 100 for L, and 1 for M. These coefficients were manually-tuned to achieve a balance between minimizing S while keeping the motions smooth and predictable. Demonstration motions and grasp locations which are typical for removal of the PPE components were provided to the algorithm by the authors in order to synthesize the robot's motions (using the process in Fig. 2).

C. Human Model and Metric Assessment

We set up the human model for each task as follows: we first take measurements of of the subject's height, shoulder width, and arm length, and create an anatomically similar human model. For the goggles and faceshield removal tasks, we put an extra rigid block on top of the model's head. This block serves as an extra obstacle TrajOpt has to avoid to be

Task	$\|Q_h\|$	# Robot Manipulators	Gripper Type	$\|Q_r\|$
Apron	18	2	Parallel-jaw	14
Faceshield	18	1	Suction	7
Goggles	18	1	Suction	7
Hood	18	2	Parallel-jaw	7
Coverall	0	2	Parallel-jaw	7

TABLE I: Human and robot DOF for the five tasks

clear of the subject's head. Finally, we set the active DoFs of the human model to be the entire body except for the coverall removal. We also include an XYZ translation joint at the feet of the human model to move it along the ground. This is to avoid having to plan footsteps and balance for the support motions. We did not plan support motions for the coverall because the only way to remove it was a sequence of transfer and support motions, so the robot is assumed to be static. See Table I for details about each task setup.

To assess risk, we used point cloud data collected from the Kinect sensor at 30Hz to track the hands and face of each subject during the doffing of the five specified PPE components. We give each execution a score using Equation 2. To assess effort, we used the recordings from the audio-visual camera (60Hz) and manually scored the posture in each frame using Equation 3.

D. Experiment results

For each subject we tested both transfer and support variants of the assisted tasks. For the analysis we took the variant with the better (lower) hands-to-face distance score from the trials and used its corresponding effort score.

Figure 4 shows snapshots from typical executions of each robot-assisted task using transfer motions. Figure 5(a) shows that the robot-assisted doffing outperformed the unassisted doffing in three out of the four infection-risk tasks (i.e. reducing the hands-to-face distance score on average). We do not consider coverall doffing as an infection-risk task because it is removed using the inner gloves, which are assumed to be uncontaminated. It is clear that the unassisted hood doffing is safer than its robot-assisted counterpart. This is because in the unassisted doffing, the subject grasps the hood from the top of his or her head, which naturally minimizes hands-to-face distance score. In contrast, the robot-assisted doffing of the hood requires the subject to grasp the lower fringes of the hood, which are closer to the face than the top part. It can also be seen that there is more variation in the hands-to-face-distance scores in the faceshield and hood assisted doffing. Both tasks required the subject to properly adjust the respective PPE components for the robot to achieve a secure grasp. Faceshield: The subject had to hold the faceshield in place using the bottom lip of the shield so that the vacuum gripper had a flat surface for successful suction. Hood: Subjects found it difficult to place the fringes onto the grippers as adjusting the hood blocked their line of sight. Thus much of the placement was done by touch.

Figure 5(b) shows that assisted doffing required less effort (on average) compared to unassisted doffing for all the tasks. Although assisted doffing takes significantly more time, it required less movement of the subjects. Assisted doffing tends to bias the subject's movements toward either the trunk

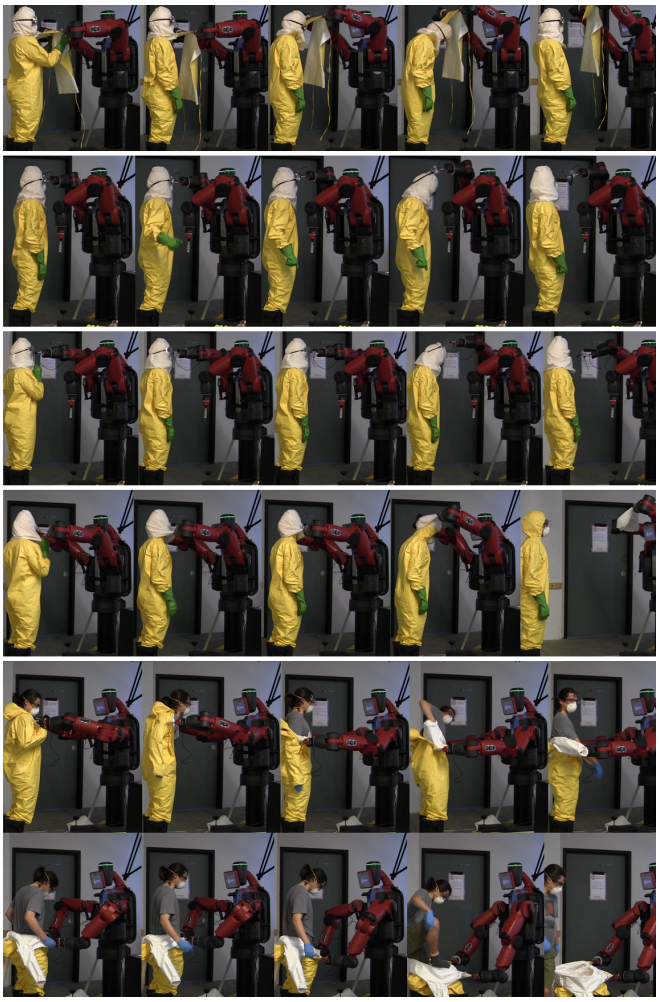

Fig. 4: Robot-Assisted doffing using transfer motions. Top-to-bottom: Apron, Goggles, Faceshield, Hood, Coverall.

or arm regions. This leaves either the trunk region exerting little to no effort during arm motions and vice-versa, which places most of the assisted doffing effort scores below ϵ_e (hence the zero scores for the apron, goggles, faceshield, and hood tasks). Four out of five of the unassisted doffing tasks required the subject to remove something by passing it over their head using their arms. These tasks produced postures wherein the torso and neck were bent and the arms were at full extension, entailing high effort scores. For the coverall, the bend-down motion subjects had to execute in order to remove the PPE during unassisted doffing produced very large increases in the effort score. In contrast, with Baxter holding down the coverall, the subjects did not need to bend down and grab the PPE.

VIII. Conclusion

We hypothesized that using a semi-autonomous robot assistant during the doffing of PPE would reduce the risk and strenuousness of the doffing procedure. We proposed a framework which takes an existing, human-only doffing demonstration and synthesizes human and robot motions to produce a robot-assisted version of the task. We then tested our framework using human subject trials with subjects

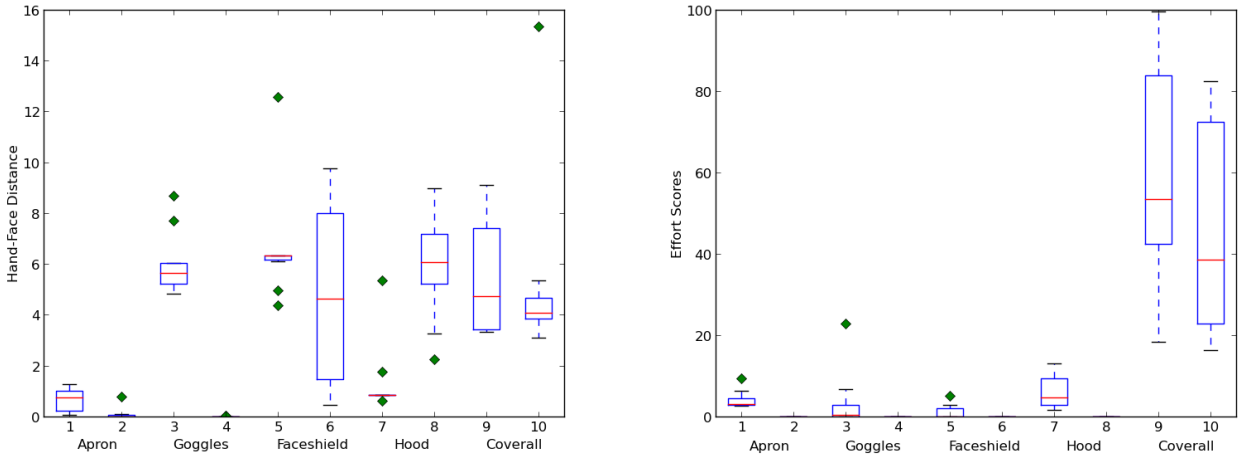

(a) Hands-to-Face Distance Score (Lower is Better)

(b) Effort Score (Lower is Better)

Fig. 5: Box plots showing the assisted vs. unassisted hands-to-face distance score and effort scores for the PPE doffing tasks. Each column represents data from 10 trials, one from each subject. The odd-numbered columns show the data for unassisted doffing, while the even-numbered columns show the data for the robot-assisted doffing. The red horizontal lines are the means for each score, the blue represent the quadrants, and the green diamonds are outliers.

performing both unassisted and assisted doffing of PPE. Our experiments with 10 subjects suggest that for the majority of PPE components which were removed with the help of a robot assistant, one or both of either infection risk and/or effort exerted were reduced in the robot-assisted variant of the procedure. However, further experiments are required to ensure the statistical significance of these results.

REFERENCES

[1] "Center for disease control and prevention. guidance on personal protective equipment (ppe)..." [Online]. Available: http://www.cdc.gov/vhf/ebola/healthcare-us/ppe/guidance.html

[2] L. McAtamney and E. Corlett, "Rula: A survey method for the investigation of work-related upper limb disorders," *Applied Ergonomics*, vol. 24, pp. 91–99, 1993.

[3] S. Hignett and L. McAtamney, "Rapid entire body assessment: Reba, applied ergonomics," *Applied Ergonomics*, vol. 31, pp. 201–205, 2000.

[4] R. Bemelmans, G. Gelderblom, P. Jonker, and L. Witte, "Socially assistive robots in elderly care: A systematic review into effects and effectiveness," in *JAMDA*, 2012.

[5] K. Yamazaki, R. Ueda, S. Nozawa, Y. Mori, T. Maki, N. Hatao, K. Okada, and M. Inaba, "A demonstrative research for daily assistive robots on tasks of cleaning and tidying up rooms," in *Proceedings of the 14th Robotics Symposia*, 2009.

[6] W. Sheng, A. Thobbi, and Y. Gu, "An integrated framework for human–robot collaborative manipulation," vol. 45, pp. 2030–2041, 2014.

[7] Y. Gao, H. Chang, and Y. Demiris, "User modelling for personalised dressing assistance by humanoid robots," in *IROS*, 2015.

[8] A. Clegg, J. Tan, G. Turk, and K. Liu, "Animating human dressing," in *SIGGRAPH*, 2015.

[9] D. Shinohara, T. Matsubara, and M. Kidode, "Learning motor skills with non-rigid materials by reinforcement learning," in *ROBIO*, 2011.

[10] D. Shinohara, M. Kidode, and T. Matsubara, "Reinforcement learning of a motor skill for wearing a t-shirt using topology coordinates," *Advanced Robotics*, vol. 27, pp. 513–524, 2013.

[11] K. Yamazaki, R. Oya, K. Nagahama, K. Okada, and M. Inaba, "Bottom dressing by a dual-arm robot using a clothing state estimation based on dynamic shape changes," *Advanced Robotic Systems*, vol. 13, 2016.

[12] B. D. Argall, S. Chernova, M. Veloso, and B. Browning, "A survey of robot learning from demonstration," *Robotics and Autonomous Systems*, vol. 57, no. 5, pp. 469 – 483, 2009.

[13] J. Nakanishi, J. Morimoto, G. Endo, G. Cheng, S. Schaal, and M. Kawato, "Learning from demonstration and adaptation of biped locomotion," *Robotics and Autonomous Systems*, vol. 47, no. 2–3, pp. 79 – 91, 2004.

[14] C. Fernandez, M. A. Vicente, R. P. Neco, and R. Puerto, "Robot grasp learning by demonstration without predefined rules," *International Journal of Advanced Robotic Systems*, vol. 8, no. 5, 2011.

[15] J. Schulman, J. Ho, A. Lee, I. Awwal, H. Bradlow, and P. Abbeel, "Finding locally optimal, collision-free trajectories with sequential convex optimization," in *RSS*, 2013.

[16] J. J. Kim and J. J. Lee, "Trajectory optimization with particle swarm optimization for manipulator motion planning," *IEEE Transactions on Industrial Informatics*, vol. 11, pp. 620–631, 2015.

[17] N. A. Vien and M. Toussaint, "POMDP Manipulation via Trajectory Optimization," in *IROS*, 2015.

[18] D. Berenson, "Manipulation of deformable objects without modeling and simulating deformation," in *IROS*, November 2013.

[19] M. Liao, Q. Zhang, W. H., R. Yang, and M. Gong, "Modeling deformable objects from a single depth camera," in *ICCV*, 2009.

[20] F. Faure, G. B., and D. Bousquet, G. Pai, "Sparse meshless models of complex deformable solids," in *SIGGRAPH*, 2011.

[21] K. Sundaraj, C. Mendoza, and C. Laugier, "A fast method to simulate virtual deformable objects with force feedback," in *ICARCV*, 2002.

[22] E. G. Gilbert, D. W. Johnson, and S. S. Keerthi, "A fast procedure for computing the distance between complex objects in three-dimensional space," *IEEE Journal on Robotics and Automation*, vol. 4, no. 2, pp. 193–203, Apr 1988.

[23] N. Vahrenkamp, T. Asfour, G. Metta, G.and Sandini, and D. R., "Manipulability analysis," in *Humanoids*, 2012.

[24] A. Dragan, K. Lee, and S. Srinivasa, "Legibility and predictability of robot motion," in *Human-Robot Interaction*, 2013.

[25] A. Dragan and S. Srinivasa, "Generating legible motion," in *RSS*, 2013.

[26] J. Cortés and T. Siméon, "Sampling-based motion planning under kinematic loop-closure constraints," *WAFR*, 2005.